European Congress on Computational Methods in Applied Sciences and Engineering
ECCOMAS 2000
Barcelona, 11-14 September 2000

THEORETICAL AND COMPUTATIONAL ISSUES IN LOCALISATION AND FAILURE

René de Borst

Koiter Institute Delft / Faculty of Aerospace Engineering
Delft University of Technology, The Netherlands
e-mail: R.deBorst@LR.TUDelft.nl

Keywords: Failure, fracture, instability, localisation, plasticity, damage, higher-order continuum, shear bands

Abstract. *An overview is given of theoretical and computational issues regarding localisation and failure phenomena in solids. Starting from an elementary one-dimensional bar problem, a classification is given of various instability phenomena. Cohesive zone models as well as enrichment of continua using gradients in space and in time are considered.*

1 INTRODUCTION

Prevention of failure of structures and structural components has always been a major concern in engineering. While there are many possible causes for structural failure, much attention has been given over the past few years to fracture of materials. Upon a closer observation of a fracture, it appears that it is often preceded by the formation of a process zone in which damage and other inelastic effects accumulate and, accordingly, in which high strain gradients prevail. This phenomenon is commonly denoted as *strain localisation*, and has been documented for a wide range of materials, for instance by Nadai as early as in 1931 in his monograph *Plasticity*[1]. Indeed, strain localisation occurs in the form of shear banding in soils, necking and the coalescence of voids in metals, rock faults, crazes in polymers and the localised accumulation of microcracks in concrete and rocks under low confining pressures.

The first theoretical contribution probably goes back to Hadamard[2] in the beginning of the previous century. After a dormant period of some fifty years theoretical considerations for strain localisation, and in fact, more generally for *material instability phenomena* were published by Hill[3], Mandel[4], Thomas[5] and Rice[6]. While attention was initially focused on localisation phenomena in metals, recently also much work has been devoted to shear banding and diffuse bifurcation modes (such as bulging) in geological materials[7], to (micro)-cracking in concrete[8,9] and to the propagation of necks in polymers[10].

Attempts to capture shear bands, cracks and other localisation phenomena via numerical methods have started in the mid-1980s. These attempts failed in the sense that the solution appeared to be determined fully by the fineness and the direction of the discretisation. The underlying reason appeared to be a local change of character of the governing equations. In the static case the elliptic character of the set of partial differential equations is lost, while, on the other hand, in the dynamic case we typically observe a change of a hyperbolic set into an elliptic set. In either case the rate boundary value problem becomes ill-posed and numerical solutions suffer from spurious mesh sensitivity.

The inadequacy of the standard, rate-independent continuum to model zones of localised straining correctly can be viewed as a consequence of the fact that force-displacement relations measured in testing devices are simply mapped onto stress-strain curves by dividing the force and the elongation by the original load-carrying area and the original length of the specimen, respectively. This is done without taking into account the changes in the micro-structure. Therefore, the mathematical description ceases to be a meaningful representation of the physical reality.

To solve this problem one must either introduce additional terms in the continuum description which reflect the changes in the micro-structure, or one must take into account the viscosity of the material[11]. In either case the effect is that the governing equations do not change type during the loading process and that physically meaningful solutions are obtained for the entire loading range. Another way to look upon the introduction of additional terms in the continuum description is that the Dirac distributions for the strain at failure are replaced by continuous strain distributions, which lend themselves for incorporation in standard numerical schemes. Although the strain gradients are now finite, they are very steep and the concentration of strain in a small area can still be referred to as strain localisation or localisation of deformation.

Along a different line solutions have been proposed in which the Dirac distribution in the strain field is incorporated in the kinematics of the finite element[12-15]. Major improvements have been reported, although, curiously, a real discontinuity is not modelled because the added strain modes are condensed at element level.

In this contribution we will start examining the by now classical example of a simple bar in pure tension, which has a small imperfection. The analytical solution will be briefly recapitulated which shows the strong mesh sensitivity and the convergence of the energy dissipation of the failure process to a zero value upon mesh refinement. To illustrate that this unphysical behaviour pertains also to more complicated boundary value problems a carbon-fibre reinforced silicium-carbide specimen is analysed. The observations that come out of the analyses for this specimen are not basically different. A popular solution is the introduction of so-called ‘cohesive zones’. In fact, finite element models with embedded discontinuities[12-15] as described above, can be conceived as refined cases of the cohesive-zone approach.

Then, the treatment will become more fundamental as underlying mathematical reasons for the strong mesh sensitivity in softening solids will be treated, as well as remedies such as the addition of spatial or temporal gradients. Using the simple framework of small-strain plasticity a classification will be given of various types of material instabilities, with emphasis on the distinction between static and propagative localisation phenomena. Also, the role of the addition of spatial or temporal gradients will be highlighted. Finally, we will focus on a framework for gradient-enhanced coupled plastic-damage theories.

2 FAILURE COMPUTATIONS

The essential shortcomings of the conventional approach as well as the properties of some remedies that have been suggested are best demonstrated by the example of a simple bar loaded in uniaxial tension, Figure 1.

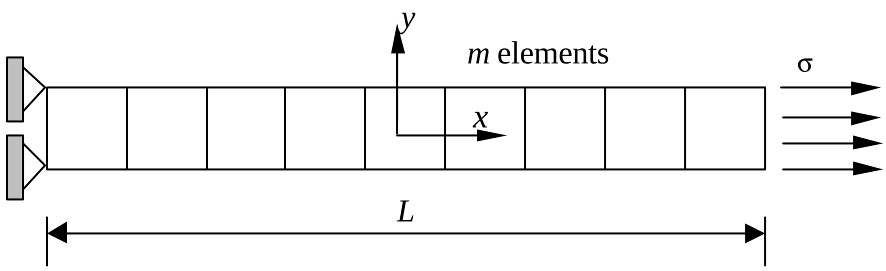

Figure 1. Bar with length L subjected to an axial stress s.

Let the bar be divided into m elements. Prior to reaching the tensile f_t a linear relation is assumed between the normal stress σ and the normal strain ε :

$$\sigma = E\varepsilon \tag{1}$$

with E Young's modulus. After reaching the peak strength a descending slope is defined in this diagram through an affine transformation from the measured load-displacement curve.

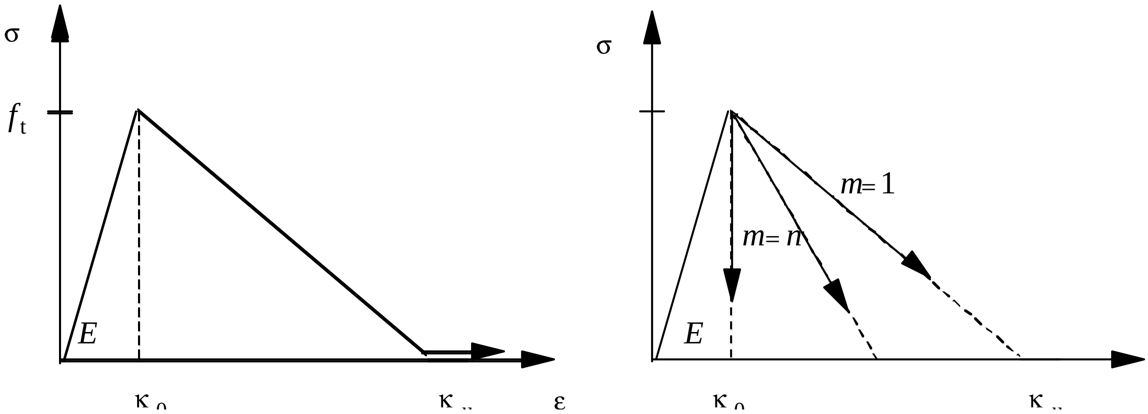

Figure 2. Left: linear softening diagram. Right: response of 1D bar for different discretisations.

The result is given in the left part of Figure 2, where κ_u marks the point where the load-carrying capacity is exhausted. In the post-peak regime the stress-strain relation thus reads:

$$\sigma = f_t + h\left(\varepsilon - \kappa_0\right), \tag{2}$$

with h the hardening/softening modulus. For linear softening we have

$$h = -\frac{f_t}{\kappa_u - \kappa_0} \ . \tag{3}$$

We now suppose that one element has a tensile strength that is marginally below that of the other m - 1 elements. Upon reaching the tensile strength of this element failure will occur. In the other, neighbouring elements the tensile strength is not exceeded and they will unload elastically. Beyond the peak strength the average strain in the bar is then given by:

$$\bar{\varepsilon} = \frac{\sigma}{E} + \frac{E-h}{Eh}\,\frac{\sigma - f_t}{m} \ . \tag{4}$$

Substitution of expression (3) for the softening modulus h and introduction of n as the ratio between the strain κ_u at which the residual load-carrying capacity is exhausted and the threshold damage level κ_0, $n = \kappa_u / \kappa_0$ and $h = -E/(n-1)$, gives

$$\bar{\varepsilon} = \frac{\sigma}{E} + \frac{n\left(f_t - \sigma\right)}{mE} \ . \tag{5}$$

This result has been plotted in the right part of Figure 2 for different ratios of n/m. The results do not seem to converge to a ‘true’ post-peak failure curve. In fact, they do converge, because the governing equations predict the failure mechanism to be a line crack with zero thickness. The numerical solution simply tries to capture this line crack, which results in localisation in one element, irrespective of the width of this element. The result on the load-average strain curve is obvious: for an infinite number of elements $(m \to \infty)$ the post-peak curve doubles back on the original loading curve. A major problem is now that, since in continuum mechanics the constitutive model is normally phrased in terms of a *stress-strain* law and not as a *force-displacement* relation, the energy that is dissipated tends to zero upon mesh refinement because the area in which the failure process occurs also becomes zero. From a physical point of view this is unacceptable

The above observations are by no way exclusive to the simple one-dimensional example quoted above. A somewhat more complicated boundary value problem is the silicium-carbide specimen of Figure 3 which is reinforced with carbon fibres (SiC/C composite). The dimensions of the specimen are 30 mm x 30 mm and a uniform horizontal loading is applied to the vertical sides. The fibres are assumed to remain elastic and also the bond between fibres and matrix material is assumed to be perfect. A softening effect is only considered for the matrix material, for which a simple Von Mises plasticity model with linear softening has been adopted[16]. A plane-strain condition has been enforced and linear elements have been used.

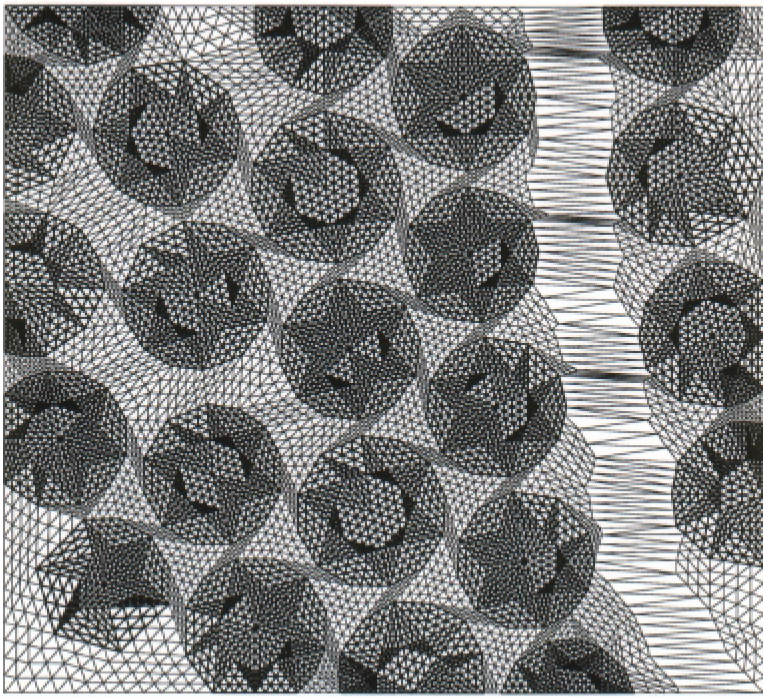

Figure 3. Deformed SiC/C specimen beyond peak load with localisation band (for finest discretisation).

After the onset of softening a clear localisation zone develops, as is shown in Figure 3. This figure actually shows the finest mesh which has 973 elements. The computed load-displacement curve has been plotted in Figure 4, together with those for the two coarser meshes, with 3892 and 15568 elements, respectively. The same picture arises as for the simple one-dimensional bar example: a more brittle response ensues if the mesh is refined, which seems to converge to a zero-energy dissipation. In fact, the solution not only becomes more brittle upon mesh refinement, also the peak load is reduced. Moreover, the solution becomes numerically very unstable when finer meshes are employed. This becomes apparent from the rather irregular shape of the load-displacement curve for the finest mesh, which could not be continued at some stage in the loading process, no matter how sophisticated solution techniques (e.g., with indirect displacement control and including line-searches) were employed. The explanation for this phenomenon is that, as shown in the simple bar problem, a refinement of the discretisation introduces more and more possible equilibrium states. The iterative solution process has to `choose' between these alternative equilibrium states and tends to pick another equilibrium state at every new iteration. Ultimately, this leads to divergence of the iterative procedure.

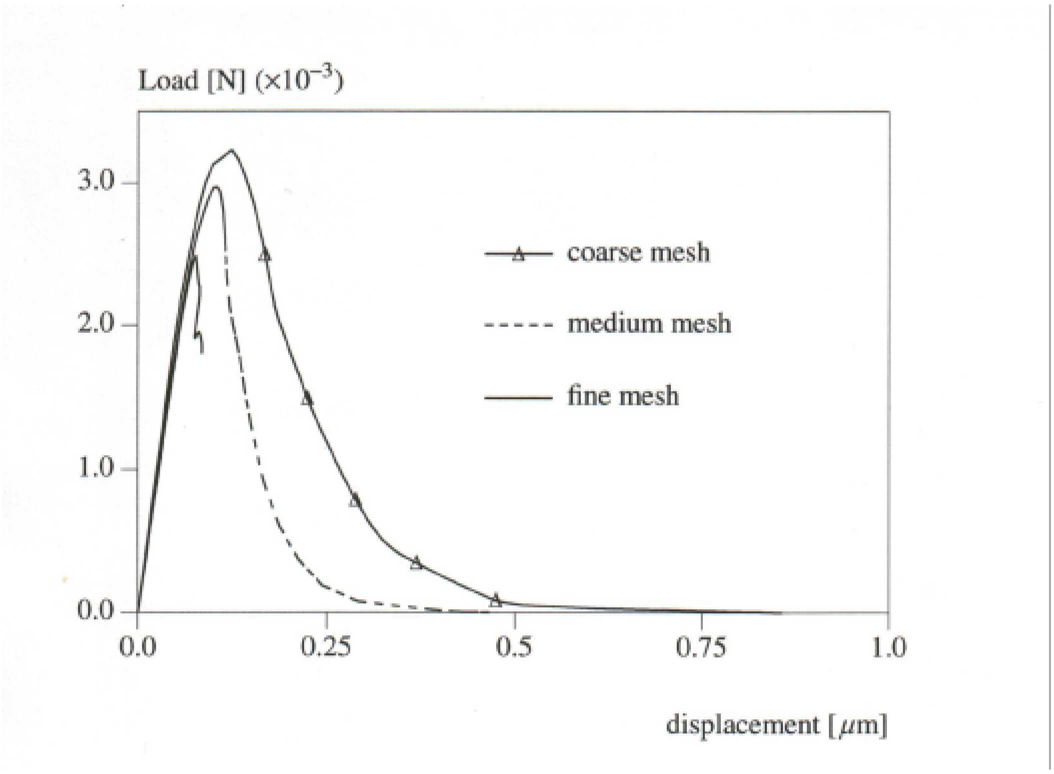

Figure 4. Load-displacement curves for the three discretisations of SiC/C specimen.

3 COHESIVE-ZONE MODELS

A most important issue when considering failure of materials is the observation that most engineering materials are not perfectly brittle in the Griffith sense, but display some ductility after reaching the strength limit. In fact, there exists a small zone in front of the crack tip, in which small-scale yielding, micro-cracking or void growth and coalescence take place. If this so-called *fracture process zone* is sufficiently small compared to the structural dimensions, linear-elastic fracture mechanics tools still apply. However, if this is no longer the case, the cohesive forces that exist in this fracture process zone must be taken into account, and so-called *cohesive-zone models* must be utilised. In such models the degrading mechanisms in front of the crack tip are lumped into a discrete line, and a stress-displacement $(\sigma - u)$ diagram over this line represents the softening effects in the fracture process zone. Apart from the shape of the stress-displacement relation, also the area under it is material-dependent. This area represents the energy that is needed to create a unit area of a fully developed crack. It is commonly called the fracture energy (G_f) and has the dimension of J/m^2 (or, equivalently, N/m). Often, only the part to the right of the damage threshold κ_0 is included in the definition of the fracture energy in order to avoid a dependency on the value of the elastic properties (i.c. Young's modulus), but this seems somewhat artificial as it excludes possible nonlinear elastic effects. Formally the definition of the fracture energy reads:

$$G_f = \int \sigma \, du \, , \tag{6}$$

with σ and u the stress and displacement across the fracture process zone. Cohesive zone models were introduced around 1960 by Barenblatt[17] and Dugdale[18] for elastic-plastic fracture in ductile metals. Probably motivated by this approach, Hillerborg[19] published his so-called Fictitious Crack Model for concrete, which ensured a mesh-independent energy release upon crack propagation.

Adapting this concept to smeared formulations, Bažant and Oh[20] developed the Crack Band Model, in which the fracture energy G_f was smeared out over the width of area in which the crack *localises*, so that

$$G_\mathrm{f} = \int \sigma\,\varepsilon(s)\,\mathrm{d}s\ . \tag{7}$$

Carrying out the integration of eq. (7) for a linear softening diagram, and assuming that the strains are constant over a band width w (an assumption commonly made in numerical analyses), we arrive at the following relation between the strain κ_u at which the residual strength is exhausted, and G_f.

$$\kappa_\mathrm{u} = \frac{2G_\mathrm{f}}{f_\mathrm{t} w}\ . \tag{8}$$

Making use of the observation that $w = L/m$, with L the length of the bar, the expression for the softening modulus h becomes:

$$h = -\frac{Lf_\mathrm{t}^2}{2mG_\mathrm{f} - Lf_\mathrm{t}^2/E}\ . \tag{9}$$

We observe that this pseudo-softening modulus is proportional to the structural size and inversely proportional to the number of elements. In fact, a model in which the softening modulus is made a function of the element size was proposed first by Pietruszczak and Mròz[21], but without resorting to an energy concept.

We shall now carry out an analysis for the tension bar of Figure 1 and give one element a tensile strength marginally below the other elements. As with the stress-based fracture model the average strain in the post-peak regime is given by eq. (4). However, substitution of the fracture-energy based expression for the pseudo-softening modulus h, eq. (9), now results in:

$$\bar{\varepsilon} = \frac{\sigma}{E} + \frac{2G_\mathrm{f}(f_\mathrm{t} - \sigma)}{Lf_\mathrm{t}^2}\ . \tag{10}$$

We observe that, in contrast to the pure stress-based fracture model, the number of elements has disappeared from the expression for the ultimate average strain. Therefore, inclusion of the fracture energy G_f as a material parameter has made the stress-average strain curves, or alternatively, the load-displacement curves, insensitive with regard to mesh refinement. But also the specimen length L has entered the expression for $\bar{\varepsilon}$. In other words, the brittleness of the structure now depends upon the value of L, so that, effectively, a size effect is introduced. Indeed, for large values of L the second term of eq. (10) which is always non-negative, approaches zero. $\bar{\varepsilon}$ becomes smaller and smaller and in the limiting case that $L \to \infty$, $\bar{\varepsilon} \to \sigma/E$, which means that the stress-average strain curve doubles back on its original loading branch.

When we prescribe the fracture energy G_f as an additional material parameter the global load-displacement response thus becomes rather insensitive of the discretisation. In finite element calculations the crack localises in a band that is one or a few elements wide, depending on the element type, the element size, the element shape and the integration scheme. Typically, it is assumed that the width over which the fracture energy is distributed can be related to the area of an element[22,23]

$$h = \alpha \sqrt{A_e} = \alpha \sqrt{\sum_{i=1}^{NINT} w_i \det \mathbf{J}_i} \ , \tag{11}$$

with w_i the weight factors of the Gaussian integration rule and $\det \mathbf{J}_i$ the Jacobian of the transformation between the local, isoparametric coordinates and the global coordinate system at integration point *i*.The factor α is a modification factor which is equal to one for quadratic elements and equal to $\sqrt{2}$ for linear elements.

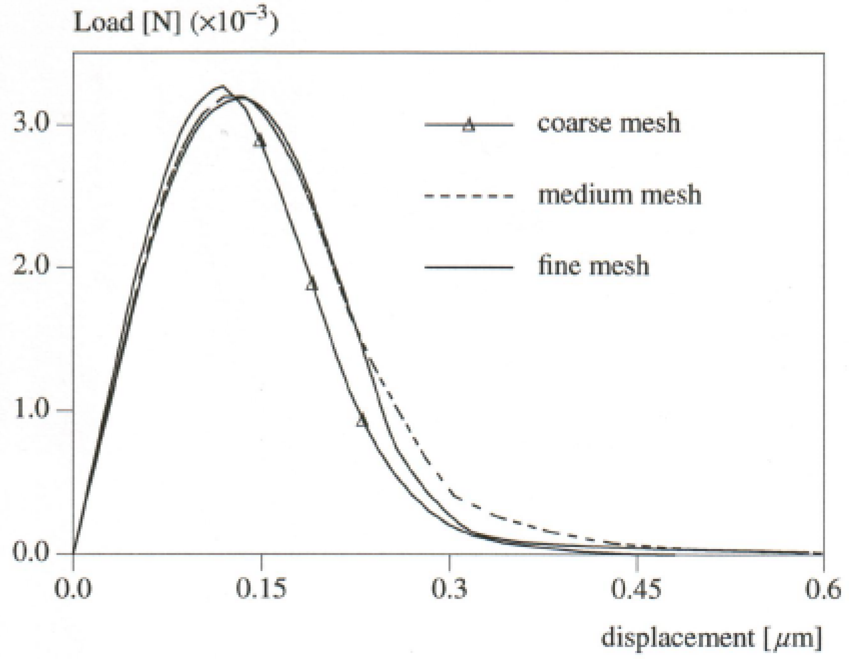

Figure 5. Load-displacement curves for SiC/C specimen with a cohesive zone model.

Recently, cohesive-zone models have become quite popular, not only for describing crack propagation in concrete and rock, but also for describing delamination and other separation effects in composites and bi-materials[16,24,25], and for fracture in metals and polymers[26]. When an *embedded* fracture process zone model, like the Crack Band Model, is applied to the SiC/C specimen that was introduced before, we indeed obtain load-displacement responses that are fairly independent of the discretisation, see Figure 5. However, it is emphasised that the number of alternative equilibrium states is not reduced. The numerical procedure is only more stable, because the softening branches are more ductile for the finer meshes because of the introduction of a fracture energy. Indeed, if one would try to include the possibility of debonding at the fibre-matrix interfaces, the number of alternative equilibrium states would increase again, and probably to such an extent that divergence again results.

4 STATIONARY AND PROPAGATIVE INSTABILITIES

Descending branches in the equivalent stress-strain diagram (softening) and non-symmetries of the tangential operator (e.g., in non-associated plasticity) are the principal sources of localisation phenomena on which numerical research has focused so far. They are called static instabilities, because the localised strain mode remains confined to a certain area in the body. However, experimental observations have revealed also other types of instabilities, like patterning in rock masses and salt formations and propagative or dynamic instabilities like Lüders bands and Portevin-Le Chatelier bands in metals and alloys, where the shear band propagates through the body. The latter type of instabilities are caused by rehardening phenomena and by a negative strain-rate sensitivity, respectively.

For a classification of instability problems[27] we shall consider the simple problem of a uniaxially stressed tensile bar. Then, the governing equations for motion and continuity can be stated in a rate format as

$$\frac{\partial \dot{s}}{\partial x} = r \, \frac{\partial^2 n}{\partial t^2} \ , \tag{12}$$

and

$$\dot{e} = \frac{\partial n}{\partial x} \quad , \tag{13}$$

in which r is the mass density and $n = \dot{u}$ the velocity. In classical small-strain plasticity, the strain rate $\dot{e}$ is additively decomposed into an elastic contribution $\dot{e}^{\mathrm{e}}$ and a plastic contribution $\dot{e}^{\mathrm{p}}$:

$$\dot{e} = \dot{e}^{\mathrm{e}} + \dot{e}^{\mathrm{p}} \tag{14}$$

Assuming linear elasticity the elastic contribution is related to the stress rate $\dot{s}$ in an bijective fashion according to

$$\dot{s} = E \, \dot{e}^{\mathrm{e}} \tag{15}$$

with E the Young's modulus. Differentiation of eq. (12) with respect to the spatial coordinate x and substitution of eqs (13)-(15) results in

$$\frac{\partial^2 \dot{s}}{\partial x^2} - \frac{r}{E} \frac{\partial^2 \dot{s}}{\partial t^2} = r \, \frac{\partial^2 \dot{e}^{\mathrm{p}}}{\partial t^2} \ . \tag{16}$$

In standard, rate-independent plasticity the stress s is purely a function of the plastic strain e^{p}: $s = s\left(e^{\mathrm{p}}\right)$. As alluded to in the Introduction, the proper description of instability phenomena requires the inclusion of gradients, either in space or in time. Accordingly, we postulate a dependence of the stress on the plastic strain, the plastic strain rate, and, following arguments advocated by Aifantis and colleagues[28-30], the second gradient of the plastic strain:

$$s = s\left(e^{\mathrm{p}}, \dot{e}^{\mathrm{p}}, \frac{\partial^2 e^{\mathrm{p}}}{\partial x^2} \right) . \tag{17}$$

In a rate format we then obtain:

$$\dot{s} = h\,\dot{e}^{\mathrm{p}} + s\,\ddot{e}^{\mathrm{p}} + g\,\frac{\partial^2 \dot{e}^{\mathrm{p}}}{\partial x^2} \quad , \tag{18}$$

with

$$h = \frac{\partial s}{\partial e^{\mathrm{p}}}\,, \qquad s = \frac{\partial s}{\partial \dot{e}^{\mathrm{p}}}\,, \qquad g = \frac{\partial s}{\partial\left(\partial^2 e^{\mathrm{p}} / \partial x^2\right)}\,. \tag{19}$$

Herein, h, s and g refer to the strain hardening/softening, the strain rate sensitivity and the gradient parameters, respectively. In general, they can be strain and strain rate dependent. We now combine eq. (16) with the constitutive equation in rate format (18), to obtain:

$$h\,\tilde{\nabla}\dot{e}^{\mathrm{p}} + s\,\tilde{\nabla}\ddot{e}^{\mathrm{p}} + g\,\tilde{\nabla}\left(\frac{\partial^2 \dot{e}^{\mathrm{p}}}{\partial x^2}\right) = r\,\frac{\partial^2 \dot{e}^{\mathrm{p}}}{\partial t^2} \quad , \tag{20}$$

with

$$\tilde{\nabla} = \frac{\partial^2}{\partial x^2} - \frac{r}{E}\,\frac{\partial^2}{\partial t^2} \quad . \tag{21}$$

To investigate the stability of the equilibrium state, we assume a harmonic fluctuation $\dot{e}^{\mathrm{p}}$ starting from a state with fully homogeneous deformations:

$$\dot{\varepsilon}^{p} = A\,e^{i(k\,x + \omega\,t)} \,, \tag{22}$$

where A is the amplitude, k is the wave number and w is the eigenvalue. Substitution of eq. (22) into eq. (20) gives

$$w^3 + a\,w^2 + b\,w + c = 0 \tag{23}$$

with

$$a = \frac{h - gk^2 + E}{s}\,, \quad b = \frac{E}{r}\,k^2\,, \quad c = \frac{Ek^2}{r}\,\frac{h - gk^2}{s}\,. \tag{24}$$

According to the Routh-Hurwitz theorem all solutions $w(k)$ have a negative real part when the following conditions are fulfilled simultaneously:

$$a = \frac{h - gk^2 + E}{s} > 0, \qquad c = \frac{Ek^2}{r}\,\frac{h - gk^2}{s} > 0,$$

$$a\,b - c = \frac{Ek^2}{r}\,\frac{E}{s} > 0 \quad . \tag{25}$$

If the Routh-Hurwitz stability criterion fails to hold, an eigenvalue with real, positive part will exist, which implies that the homogeneous state is unstable and a small perturbation can grow into, for instance, a shear band instability. Thus, we have two possible types of instabilities:

(i) An h-type instability which is associated with the formation of stationary macroscopic shear bands

$$s > 0 \quad , \qquad h - g\,k^2 < 0 \tag{26}$$

It is interesting to note that the h-type instability is dependent on k, the wave number, which has a cut-off value

$$k \geq \sqrt{\frac{h}{g}} \tag{27}$$

Because the wavelength l is defined as

$$l = \frac{2p}{k} \ , \tag{28}$$

only wavelengths smaller than $2p/k$ can propagate in the shear bands. If we define $l = l/(2p)$ we obtain the internal length scale

$$l = \sqrt{\frac{g}{h}} \tag{29}$$

The thickness of a shear band in the one-dimensional case exactly matches the largest possible wavelength $l = 2p\, l$.

(ii) An s-type instability which is associated with the occurrence of travelling Portevin-Le Chatelier (PLC) bands

$$s < 0 \,, \qquad h > 0 \quad . \tag{30}$$

5 GRADIENT ENHANCED ELASTO-PLASTIC-DAMAGE THEORIES

Now, we shall extend the one-dimensional gradient plasticity model discussed in the preceding section to a three-dimensional gradient-enhanced model, in which damage is coupled to plasticity. Firstly, we shall briefly summarise the existing knowledge on gradient elastic-damage and on gradient plasticity theories. Next, the theory will be extended to damage theories, where the damage evolution is coupled to plasticity. A concise elaboration will be given of the numerical implementation.

Below we shall first outline the structure of the elasticity-based gradient damage theory developed by Peerlings et al[31-33]. The basic stress-strain relation is given by

$$\boldsymbol{s} = (1 - \omega)\, \mathbf{D}^{e} : \boldsymbol{e} \tag{31}$$

with σ the stress tensor, $\mathbf{D}^{e}$ the virgin Hookean stiffness matrix, $\boldsymbol{e}$ the strain tensor and ω a scalar-valued damage variable, starting at 0 for undamaged material and reaching 1 upon complete disintegration of the material. The damage variable is a function of the strain state through a scalar-valued history parameter κ^{d},

$$\omega = \omega\left(\kappa^{d}\right) \tag{32}$$

where κ^{d} obeys a loading function f^{d},

$$f^{d} = \bar{\varepsilon} - \kappa^{d} \tag{33}$$

with $\bar{\varepsilon}$ a non-standard equivalent strain which is coupled to the standard, local equivalent strain $\tilde{\varepsilon}$ via a Helmholtz-type equation

$$\bar{\varepsilon} - g\nabla^{2}\bar{\varepsilon} = \tilde{\varepsilon} \tag{34}$$

with g the gradient parameter and $\tilde{\varepsilon}$ a function of the strain tensor $\boldsymbol{e}$.

Plasticity theories differ from elasticity-based damage theories in the sense that a decomposition is assumed with respect to the strain. For the small-strain flow theory of plasticity this decomposition directly applies to the rates:

$$\dot{\boldsymbol{e}} = \dot{\boldsymbol{e}}^{\mathrm{e}} + \dot{\boldsymbol{e}}^{\mathrm{p}}. \tag{35}$$

The elastic part is coupled to the stress rate $\dot{\boldsymbol{s}}$ via Hooke's relation, *cf* eq (31):

$$\dot{\boldsymbol{s}} = \mathbf{D}^{\mathrm{e}} : \boldsymbol{e}^{\mathrm{e}} \tag{36}$$

The plastic strain rates are commonly derived from a plastic potential function, Φ, as follow:

$$\dot{\boldsymbol{e}}^{\mathrm{p}} = \dot{\varepsilon}^{\mathrm{p}} \frac{\partial \Phi}{\partial \boldsymbol{s}} \tag{37}$$

with $\dot{\varepsilon}^{\mathrm{p}}$ the equivalent plastic strain rate. Its magnitude follows from enforcing the consistency condition $\dot{f}^{\mathrm{p}} = 0$, where in a gradient-plasticity theory the plastic loading function f^{p} is defined by[28-30,34]:

$$f^{\mathrm{p}} = \tilde{\sigma} - \bar{\kappa} \tag{38}$$

with $\tilde{\sigma}$ a function of the stress components, e.g., via the Von Mises definition, and $\bar{\kappa}$ is a functional of ε^{p} and, unlike in standard plasticity, of its Laplacian, $\nabla^2 \varepsilon^{\mathrm{p}}$. Elaboration of the consistency condition then yields a Helmholtz equation for the plastic strain rate:

$$\dot{\varepsilon}^{\mathrm{p}} + \frac{g}{h} \nabla^2 \dot{\varepsilon}^{\mathrm{p}} = -\frac{1}{h} \frac{\partial \tilde{\sigma}}{\partial \boldsymbol{s}} : \dot{\boldsymbol{s}} \tag{39}$$

quite similar to the governing equation for the non-standard total strain in an elasticity-based gradient damage theory, eq. (34). A difference is the occurrence of a hardening modulus,

$$h = -\frac{\partial \bar{\kappa}}{\partial \varepsilon^{\mathrm{p}}} \tag{40}$$

which causes that the gradient constant

$$g = -\frac{\partial \bar{\kappa}}{\partial \nabla^2 \varepsilon^{\mathrm{p}}} \tag{41}$$

has a different dimension than that in the gradient-damage theory. Another major difference is that eq. (34) is valid on the entire domain occupied by the body, whereas eq. (39) only applies to the plastified part. This has severe consequences, since now the boundary conditions must be taken care of at the elastic-plastic boundary. This is particularly difficult since this boundary is unknown and, moreover, changes throughout the loading process. In practice, this problem has been solved by utilising C^1-continuous shape functions for the interpolation of the plastic equivalent strain ε^{p}.

For the above reason, gradient damage theories are computationally more versatile than gradient plasticity formalisms. For combining both approaches it is therefore preferable to depart from a gradient-damage theory and to enrich this theory such that irreversible straining is properly accommodated. To this end we take eq. (31) as point of departure and change it into:

$$\boldsymbol{s} = (1 - \omega)\, \mathbf{D}^{\mathrm{e}} : (\boldsymbol{e} - \boldsymbol{e}^{\mathrm{p}}) \tag{42}$$

while the plastic strain rate still follows from eq. (37), but their occurrence is now governed by a strictly local plastic loading function

$$f^{\mathrm{p}} = \tilde{\sigma}\left(\hat{\boldsymbol{s}}\right) - \kappa\left(\varepsilon^{\mathrm{p}}\right) \tag{43}$$

so that the consistency relation remains a pointwise relation

$$\dot{\varepsilon}^{\mathrm{p}} = -\frac{1}{h}\frac{\partial\tilde{\sigma}}{\partial\hat{\boldsymbol{s}}} : \dot{\hat{\boldsymbol{s}}} \tag{44}$$

As is implied in eq. (43) the stress measure $\tilde{\sigma}$ is no longer a function of the stress components of $\boldsymbol{s}$. Instead, it is derived from the effective stresses

$$\hat{\boldsymbol{s}} = \frac{\boldsymbol{s}}{1-\omega} \tag{45}$$

which stems from the observation that plasticity can only apply to the intact matrix material, and not to the voids. The nonlocal aspect thus resides entirely in the averaging equation (34) for the equivalent strain ω remains a function of the damage history parameter κ^{d}, as in eq. (32).

An algorithm for this theory reads:

1. Solve for nodal displacements $\mathbf{u}$ and nodal non-standard equivalent strains $\bar{\boldsymbol{e}}$.
2. Compute strains and non-standard equivalent strains in integration points at iteration n+1 : $\boldsymbol{e}_{\mathrm{n+1}}$, $\bar{\varepsilon}_{\mathrm{n+1}}$.
3. Resolve plasticity in effective stress space:

   $\hat{\boldsymbol{s}}_0 = \boldsymbol{s}_0 / \left(1-\omega_0\right)$

   $\hat{\boldsymbol{s}}_{\mathrm{trial}} = \hat{\boldsymbol{s}}_0 + \mathbf{D}^{\mathrm{e}} : \left(\boldsymbol{e}_{\mathrm{n+1}} - \boldsymbol{e}_{\mathrm{n}}\right)$

   $\tilde{\boldsymbol{s}}_{\mathrm{trial}} = \tilde{\boldsymbol{s}}_{\mathrm{trial}}\left(\hat{\boldsymbol{s}}_{\mathrm{trial}}\right)$

   Evaluate the plastic loading function: $f^{\mathrm{p}} = \tilde{\boldsymbol{s}}_{\mathrm{trial}} - \kappa\left(\varepsilon_0^{\mathrm{p}}\right)$.

   If $f^{\mathrm{p}} > 0$: $\hat{\boldsymbol{s}}_{\mathrm{n+1}} = \hat{\boldsymbol{s}}_{\mathrm{trial}} - \Delta\varepsilon^{\mathrm{p}}\,\mathbf{D}^{\mathrm{e}} : \left(\frac{\partial\Phi}{\partial\hat{\boldsymbol{s}}}\right)_{\mathrm{n+1}}$

   using a standard return-mapping scheme, to compute $\Delta\varepsilon^{\mathrm{p}}$,

   else : $\hat{\boldsymbol{s}}_{\mathrm{n+1}} = \hat{\boldsymbol{s}}_{\mathrm{trial}}$, $\Delta\varepsilon^{\mathrm{p}} = 0$
4. Evaluate the damage loading function $f^{\mathrm{d}} = \bar{\varepsilon}_{\mathrm{n+1}} - \kappa_{\mathrm{n}}^{\mathrm{d}}$

   If $f^{\mathrm{d}} > 0$: $\kappa_{\mathrm{n+1}}^{\mathrm{d}} = \bar{\varepsilon}_{\mathrm{n+1}}$

   else : $\kappa_{\mathrm{n+1}}^{\mathrm{d}} = \kappa_{\mathrm{n}}^{\mathrm{d}}$

   Compute : $\omega_{\mathrm{n+1}} = \omega\left(\kappa_{\mathrm{n+1}}^{\mathrm{d}}\right)$
5. Transform stress: $\boldsymbol{s}_{\mathrm{n+1}} = \left(1-\omega_{\mathrm{n+1}}\right)\hat{\boldsymbol{s}}_{\mathrm{n+1}}$
6. Compute force vectors and, if no convergence has been achieved, the tangential stiffness matrices and repeat the iteration loop.

5 REFERENCES

[1] Nádai, A., *Plasticity*. McGraw-Hill, New York and London (1931).
[2] Hadamard, J., *Lecons sur la Propagation des Ondes.* Herman et fils, Paris (1903).
[3] Hill, R. A general theory of uniqueness and stability in elastic-plastic solids, *J. Mech. Phys. Solids*, **6**, 236-249 (1958).
[4] Mandel, J., Conditions de stabilité et postulat de Drucker. In: *Proc. IUTAM Symposium on Rheology and Soil Mechanics*, Springer-Verlag, Berlin (1966), pp. 58-68.
[5] Thomas, Y., *Plastic Flow and Fracture of Solids*. Academic Press, New York (1961).
[6] Rice, J.R., The localization of plastic deformation. In: *Theoretical and Applied Mechanics*, North-Holland, Amsterdam (1976), pp. 207-220.
[7] Vardoulakis, I. and Sulem, J., *Bifurcation Analysis in Geomechanics*. Blackie, London (1995).
[8] Karihaloo, B. *Fracture Mechanics and Structural Concrete.* Addison Wesley Longman, Harlow (1995).
[9] Baž ant, Z.P. and Planas, J., *Fracture and Size Effect in Concrete and Other Quasibrittle Materials*. CRC Press, Boca Raton (1998).
[10] Hutchinson, J.W. and Neale, K.W., Neck propagation, *J. Mech. Phys. Solids,* **31**, 405-426 (1983).
[11] de Borst, R., Sluys, L.J., Mühlhaus, H.-B., Pamin, J., Fundamental issues in finite element analysis of localisation of deformation, *Eng. Comput*. **10**, 99-122 (1993).
[12] Belytschko, T., Fish, J. and Engelmann, B.E., A finite element with embedded localization zones, *Comp. Meth. Appl. Mech. Eng*. **70**, 59-89 (1988).
[13] Simo, J.C., Oliver, J. and Armero, F., An analysis of discontinuities induced by strain-softening in rate-independent inelastic solids, *Comput. Mech*. **12**, 277-296 (1993).
[14] Larsson, K. Runesson and N.S. Ottosen, Discontinuous displacement approximation for capturing plastic localization, *Int. J. Num. Meth. Eng*. **30**, 541-564 (1993).
[15] Sluys, L.J. and Berends, A.H., Discontinuous failure analysis for mode-I and mode-II localization problems, *Int. J. Solids Struct*. **35**, 4257-4274 (1998).
[16] Schellekens, J.C.J., *Computational Strategies for Composite Structures*. Dissertation, Delft University of Technology, Delft (1992).
[17] Barenblatt, G.I., The mathematical theory of equilibrium cracks in brittle fracture, *Adv. Appl. Mech*. **7**, 55-129 (1962).
[18] Dugdale, D.S., Yielding of steel sheets containing slits, *J. Mech. Phys. Solids* **8**, 100-108 (1960).
[19] Hillerborg, A., Modeer, M. and Petersson, P.E., Analysis of crack formation and crack growth in concrete by means of fracture mechanics and finite elements, *Cement Concr. Res*. **6**, 773-782 (1976).
[20] Baž ant, Z.P. and Oh, B., Crack band theory for fracture of concrete, *RILEM Mat. Struct*. **16** (1983) 155-177.
[21] Pietruszczak, S. and Mróz, Z., Finite element analysis of deformation of strain softening materials, *Int. J. Num. Meth. Eng*. **17**, 327-334 (1981).

[22] Willam, K.J., Experimental and computational aspects of concrete failure. In: *Proc. Int. Conf. Computer Aided Analysis and Design of Concrete Structures* Pineridge Press, Swansea (1984), pp. 33-70.
[23] Feenstra, P.H. and de Borst, R., A plasticity model and algorithm for mode-I cracking in concrete, *Int. J. Num. Meth. Eng*. **38**, 2509-2529 (1995).
[24] Schellekens, J.C.J. and de Borst, R., Free edge delamination in carbon-epoxy laminates: a novel numerical/experimental approach, *Compos. Struct*., **28**, 357-373 (1994).
[25] Wei, Y. and Hutchinson, J.W., Models of intrface separation accompanied by plastic dissipation at multiple scales, *Int. J. Fracture* **95**, 1-17 (1999).
[26] Needleman, A., A continuum model for void nucleation by inclusion debonding, *J. Appl. Mech*. **54**, 525-531 (1987).
[27] Wang, W., *Stationary and Propagative Instabilities in Metals - A Computational Point of View*. Dissertation, Delft University of Technology, Delft (1997).
[28] Aifantis, E.C., On the microstructural origin of certain inelastic models, *Trans.ASME J. Eng. Mat. Technol*. **106**, 326-330 (1984).
[29] Mühlhaus, H.-B. and Aifantis, E.C., A variational principle for gradient plasticity, *Int. J. Solids Struct*. **28**, 845-858 (1991).
[30] de Borst, R. and Mühlhaus, H.-B., Gradient-dependent plasticity: formulation and algorithmic aspects, *Int. J. Num. Meth. Eng*. **35**, 521-539 (1992).
[31] Peerlings, R.H.J. *Enhanced Damage Modelling for Fracture and Fatigue*. Dissertation, Eindhoven University of Technology, Eindhoven (1999).
[32] Peerlings, R.H.J., de Borst, R., Brekelmans, W.A.M. and de Vree, H.P.J., Gradient-enhanced damage for quasi-brittle materials, *Int. J. Num. Meth. Eng*.**39**, 3391-3403 (1996).
[33] Peerlings, R.H.J., de Borst, R., Brekelmans, W.A.M., de Vree, H.P.J. and Spree I., Some observations on localisation in non-local and gradient damage models, *Eur. J. Mech.: A/Solids*, **15**, 937-954 (1996).
[34] de Borst. R., Pamin. J. and Geers, M.G.D., On coupled gradient-dependent plasticity and damage theories with a view to localization analysis, *Eur. J. Mech.: A/Solids*, **18**, 939-962 (1999).